IEEE Access
Multidisciplinary | Rapid Review | Open Access Journal

Received March 23, 2022, accepted April 4, 2022, date of publication April 7, 2022, date of current version April 21, 2022.

Digital Object Identifier 10.1109/ACCESS.2022.3165651

Modified Brain Emotional Controller-Based Ripple Minimization for SVM-DTC of Sensorless Induction Motor Drive

SRIDHAR SAVARAPU[1], (Senior Member, IEEE), MD. QUTUBUDDIN[2], AND YADAIAH NARRI[3], (Senior Member, IEEE)

[1]Department of Electrical and Electronics Engineering, JNTUA College of Engineering Ananthapur, Ananthapur, Andhra Pradesh 515002, India
[2]Department of Electrical and Electronics Engineering, TKR College of Engineering and Technology, Hyderabad, Telangana 500097, India
[3]Department of Electrical and Electronics Engineering, JNTUH College of Engineering, Hyderabad, Telangana 500085, India

Corresponding author: Sridhar Savarapu (ssridhar229@gmail.com)

ABSTRACT This paper presents the Modified Brain Emotional Controller (MBEC) technique for the minimization of torque and flux ripples of sensorless Induction Motor (IM) drive. In low-speed operation, IM is very sensitive due to variations in torque and flux ripples. These variations inert low order harmonics in stator currents that adversely affect the performance of the IM drive. The drive's performance can be improved by integrating a controller that not only minimizes harmonic presence but also increases the drive's performance. In this paper a biological inspired intelligent speed controller namely, MBEC is proposed to obtain improved performance from the drive. The input to the MBEC is an error of the reference speed and the actual speed of the motor that is estimated using the Model Reference Adaptive System (MRAS). SVM based topology is used to develop the inverter and IM is operated in sensorless DTC technique. Stability analysis of MBEC based IM drive is presented in this paper to hold the effectiveness. The proposed control configuration is tested with different operating conditions and obtained results are verified through real-time experimentation using Opal-RT OP5600. The performance of the proposed control algorithm is compared with the BEC and PI techniques to hold the effectiveness in terms of low flux ripples and torque ripples in different operating conditions.

INDEX TERMS Modified brain emotional controller, model reference adaptive system, sensorless IM drive, direct torque control, space vector modulation.

I. INTRODUCTION

Artificial intelligence (AI) techniques have become popular and found in wide variety of industrial applications. Brain Emotional Controller (BEC) is one of the AI techniques more suitable for applying in wide range of control engineering applications [1]–[5]. The design of BEC is inspired by the emotional system of mammalian brain using limbic system, Orbitofrontal cortex and their associative parts. In BEC there is dual learning process one in the amygdale another in the orbitofrontal cortex that involves in taking swift decisions. The learning methodology of BEC is encouraged to apply in various industrial applications.

Industrial systems are mostly dependent on Induction motors (IM) due to their advantageous features and characteristics similar to a DC motor. IM while operating in process industries, submarine systems, chemical industries, and many more sensors are absent in which the motor variables need to be estimated during this process since the internal characteristics of IM are deteriorated.

In adjustable speed drive applications [6] the performance of the IM can be improved using one of two control techniques vector control and Direct Torque Control (DTC) [7]. The vector control approach is modeled using stator currents and flux whereas DTC technique with two individual controllers using flux and torque that embedded directly. The major drawback of the vector control technique is sensitivity to motor parameters, coordinate transformation, and power regulator setup. These variations adversely affect particularly in low-speed operation of IM drive. DTC technique can overcome the drawbacks of vector control IM drive. DTC structure provides rapid dynamic response and robustness to

The associate editor coordinating the review of this manuscript and approving it for publication was Zhuang Xu.

the parameters of the rotor and has a significantly reduced inverter control structure. DTC has certain limitations such as excessive torque and flux ripples. Conventionally, the inverter topology applied in the DTC technique is based on the hysteresis band to obtain switching pulses. The prescribed band in the hysteresis controller gives limited switching pulses that affect the torque and flux ripples during the change in load and speed respectively. In [8] presented Space Vector Modulation (SVM) in DTC to minimize torque and flux ripples. SVM substitutes the hysteresis model of inverter switching with dwell time-based switching that retains the fixed frequency of switching and the effects of torque ripples on decreasing flux [9]–[12]. Though SVM-based DTC strategy gives satisfactory results, to achieve high performance from the drive, the position information of the rotor and speed information are required to get refined switching pulse to the inverter. The speed and rotor position information can be collected using a controller, the speed controller smoothens the torque component, and in turn the torque ripples are minimized.

The MRAS technique is used to estimate the speed and rotor position of IM to operate under sensorless. The configuration of MRAS contains reference and adjustable models with a controller, generally a proportional-integral (PI) controller. The estimated speed received from the MRAS is termed as the actual speed of the machine compared with the reference speed and process in to the speed controller to obtain torque information [13]–[15]. Many researchers have been developed different speed controllers namely the classical PI controllers, predictive controllers, sliding mode controllers, and AI based controllers such as fuzzy logic controllers, artificial neural networks and many more. The confined performance of the existing classical and AI based controllers switched to modern intelligent controllers that not only contain simple architecture but also easy implementation. The modern intelligent controllers can be developed using the decision-making process of a human. The limbic system is responsible for emotional behavior and to take quick decisions. In control engineering applications, Caro Lucas introduces the computational network model for limbic systems as BEC. This controller is employed in general-purpose embedded systems [16]–[19]. The BEC was implemented for PMSM drive-by M.A. Rahman *et al.* [20]. The main features of BEC are enhanced self-learning capability, provision of the model-free control algorithm, robustness, and ability to respond as a swift controller.

In this paper, by integrating the Sensory cortex into the BEC structure, the sensory signal is processed quickly and accumulated with other limbic system components, allowing for very quick intervention. In order to reach a high efficiency compared with the existing BEC, the modified BEC (MBEC) is configured to control the IM drive. Further, to get speed as a feedback signal, The MRAS approach is used in sensorless IM drive to predict rotor position and speed [21]. The proposed MBEC based AI method improves the IM drive's dynamic performance [22], [23]. In the design of speed controllers, the development of the DTC strategy, parameter variance issues, non-linear nature of the drive, and load toque disruption effects on motor efficiency are burgeoned with a broad emphasis on computational AI techniques.

They have a good dynamic performance, but when practically applied they add complexity to the architecture and need the use of fast digital signal processors to execute various controller computations [24]–[27]. Simulation and experimental findings are investigated and PI-based SVM DTC strategies evaluate the output of the proposed controller. In the hardware-in-loop mechanism, closed-loop testing of the proposed DTC strategy is carried out. The motor receives the Op-RTDS control output signals, and the Op-RTDS receives the DTC control scheme feedback signals in real time [28]–[30]. After that, the simulation and experimental synthesis take place, and the test system connects with the Op-RTDS simulation. Fig.1 shows MBEC based IM drive in which sensorless DTC technique is used to estimate the motor speed and to control the speed of IM. MBEC is applied to design the sensorless technique, the MRAS structure is adopted. The stability analysis of MBEC-IM is performed in this paper and developed the adaptive law for the estimation of motor parameters.

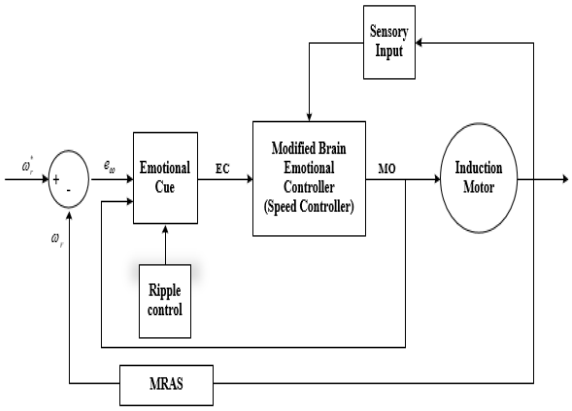

FIGURE 1. Block diagram of MBEC based IM drive.

This paper is organized as follows: Section II presents SVM DTC based sensorless IM drive and also speed estimation technique using MRAS is described here. Section III explains the development of MBEC and it is implemented in SVM DTC based sensorless IM drive. Section IV deals with stability analysis for MRAS. Section V contains the results of the experiments and test cases used to evaluate the proposed MBEC architecture in high-performance applications. Finally, in Section VI there are some conclusions.

II. SVM-DTC BASED SENSORLESS IM DRIVE

Electric drive based industry is increasing enormously that encourages to develop newer techniques to obtain high

performance. The developed techniques required to be tested on benchmark applications. The newly developed techniques cannot be applied directly on real-time models, must be evaluated in different conditions using simulation environment. In simulation, the system characteristics can be analyzed using mathematical model of the system.

In this paper, an IM drive is operated in a sensorless DTC scheme using SVM based inverter. The mathematical model of IM drive is developed initially and for sensorless operation Model Reference Adaptive System is developed later.

A. MATHEMATICAL MODELLING OF DTC BASED INDUCTION MOTOR DRIVE

The mathematical model of an IM is unique with respect to the reference frame. The mathematical model referred to as stationary reference frame is used in the DTC strategy. The impedance based induction motor is expressed in (1), shown at the bottom of the page, where,

$$I = \begin{bmatrix} 1 & 0 \\ 0 & 1 \end{bmatrix}$$

and Θ:2×2 *null matrix*

$$X_{ml}^{*} = \frac{1}{\frac{1}{X_m} + \frac{1}{X_{ls}} + \frac{1}{X_{lr}}}$$

ω_b : *motor angle base frequency*
ω_r : *rotor angular speed*
Ψ_{ds} : *stator flux linkage*
Ψ_{qs} : *stator flux linkage*
Ψ_{dr} : *rotor flux linkage*
Ψ_{qr} : *rotor flux linkage*
X_{ls} : *stator leakage reactance*
X_{lr} : *rotor leakage reactance*
X_m : *mutual reactance*
$v_{ds}v_{qs}$: *stator voltages*
$v_{dr}v_{qr}$: *rotor voltages*

In real-time, the estimated stator flux through the voltage and current signals at each sampling signal t_s the stator flux and actual stator flux can be written in the d,q components of the discrete form as in (2), (3) and (4). Using the transformation, *d-q* axis stator flux linkages at each sampling period can be obtained as in (2) and (3) these are used to estimate stator flux as given in (4)

$$\Psi_{ds}(k+1) = \Psi_{ds}(k) - t_s R_s i_{ds}(k) + t_s V_{ds}(k) \quad (2)$$

$$\Psi_{qs}(k+1) = \Psi_{qs}(k) - t_s R_s i_{qs}(k) + t_s V_{qs}(k) \quad (3)$$

$$\Psi_s(k+1) = \sqrt{\Psi_{ds}^2(k+1) + \Psi_{qs}^2(k+1)} \quad (4)$$

The torque developed in the IM is expressed as

$$T_e = \frac{3}{2}\left(\frac{p}{2}\right)\frac{L_m}{L_r L_s}\left(\vec{\Psi}_s \times \vec{\Psi}_r\right) \quad (5)$$

Using *d-q* stator flux and currents, the torque of the motor is estimated as

$$T_e(k+1) = T_e(k) - \frac{3p}{4}\left(\Psi_{ds}(k)\, i_{qs}(k) - \Psi_{qs}(k)\, i_{ds}(k)\right) \quad (6)$$

In DTC, the estimated flux in (4) and estimated electromagnetic torque in (6) are compared with reference commands. The errors of torque and flux are used to determine inverter switching states either by switching table based SVM strategy or dwell-time based SVM strategy.

B. SENSORLESS SVM-DTC BASED IM DRIVE

The MRAS structure is displayed in Fig.2. It contains two structures, one is the Reference Model (RM) and the other is an Adjustable Model (AM). An adaptive mechanism remains currently present. The error out of RM and AM are fed directly into the adaptive mechanism. The parameters from the RM are fixed and the parameter values from AM are varied, therefore the error between two models AM and RM becomes zero. MRAS is one of the most common and favored schemes for sensorless IM drives, as they are simple to implement to achieve good results.

When the speed is precisely evaluated, both the RM and AM outputs are equal to zero. Both the outputs Ψ_r^x and Ψ_r^y estimates rotor flux space vector in the stationary reference

$$\begin{bmatrix} \dot{\Psi}_{qs} \\ \dot{\Psi}_{ds} \\ \dot{\Psi}_{qr} \\ \dot{\Psi}_{dr} \end{bmatrix} = \begin{bmatrix} 0 & \frac{R_s\omega_b}{X_{ls}}\left[\frac{X_{ml}^*}{X_{ls}} - 1\right] & 0 & \frac{R_r\omega_b}{X_{lr}}\left[\frac{X_{ml}^*}{X_{ls}}\right] \\ \frac{R_s\omega_b}{X_{ls}}\left[\frac{X_{ml}^*}{X_{ls}} - 1\right] & 0 & \frac{R_r\omega_b}{X_{lr}}\left[\frac{X_{ml}^*}{X_{ls}}\right] & 0 \\ 0 & \frac{R_s\omega_b}{X_{ls}}\left[\frac{X_{ml}^*}{X_{lr}}\right] & -\omega_r & \frac{R_s\omega_b}{X_{lr}}\left[\frac{X_{ml}^*}{X_{lr}} - 1\right] \\ \frac{R_s\omega_b}{X_{ls}}\left[\frac{X_{ml}^*}{X_{lr}}\right] & 0 & \frac{R_s\omega_b}{X_{lr}}\left[\frac{X_{ml}^*}{X_{lr}} - 1\right] & -\omega_r \end{bmatrix} \begin{bmatrix} \Psi_{qs} \\ \Psi_{ds} \\ \Psi_{qr} \\ \Psi_{dr} \end{bmatrix} + \omega_b \begin{bmatrix} I & \Theta \\ \Theta & \Theta \end{bmatrix} \begin{bmatrix} v_{qs} \\ v_{ds} \\ v_{qr} \\ v_{dr} \end{bmatrix} \quad (1)$$

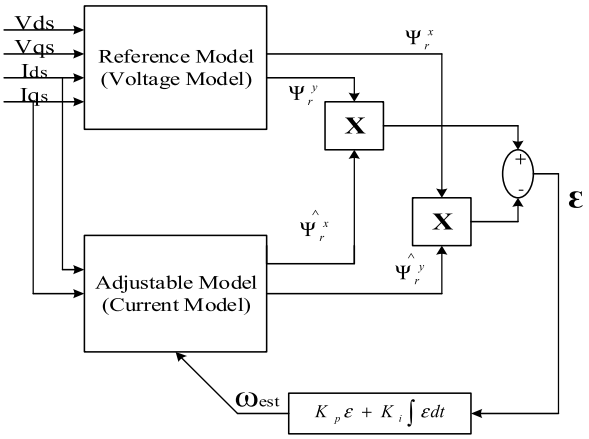

FIGURE 2. MRAS structure for speed estimation of IM drive.

frame.

$$\underline{u}_{sn} = R_s \underline{i}_n + \frac{d\underline{\Psi}_s}{dt} \tag{7}$$

$$0 = R_r \underline{i}_r + \frac{d\underline{\Psi}_r}{dt} - j\omega_r \underline{\Psi}_r \tag{8}$$

Equations for stator and rotor in the stationary frame as the rotor speed affects the computation of flux, Eqns. (7)-(8) represent the AM of Fig.2. Following are the rotor flux components as seen in the stationary reference frame

$$p\begin{bmatrix}\Psi_r^x \\ \Psi_r^y\end{bmatrix} = \frac{L_r}{L_m}\left[\begin{bmatrix}U_{sn}^x \\ U_{sn}^y\end{bmatrix} - \begin{bmatrix}(R_s+\sigma L_s\rho) & 0 \\ 0 & (R_s+\sigma L_s\rho)\end{bmatrix} \times \begin{bmatrix}i_{\alpha s} \\ i_{\beta s}\end{bmatrix}\right] \tag{9}$$

$$p\begin{bmatrix}\Psi_r^x \\ \Psi_r^y\end{bmatrix} = \begin{bmatrix}-\frac{1}{T_r} & -\omega_r \\ \omega_r & -\frac{1}{T_r}\end{bmatrix}\begin{bmatrix}\Psi_r^x \\ \Psi_r^y\end{bmatrix} + \frac{L_m}{T_r}\begin{bmatrix}i_{\alpha s} \\ i_{\beta s}\end{bmatrix} \tag{10}$$

where $\sigma = 1 - (L_m^2/L_sL_r)$ and $p = \frac{d}{dt}$ ω_r is rotor angular speed and T_r is the rotor time constant. The rotor speed estimation algorithm is adjusted by the speed tuning signal, which transforms the error signal to zero.

$$\omega^{Esti} = K_P\varepsilon + K\int \varepsilon dt \tag{11}$$

The input of the PI controller as

$$\varepsilon = \hat{\Psi}_r^x \Psi_r^y + \hat{\Psi}_r^y \Psi_r^x \tag{12}$$

The PI controller parameters are K_p and K_i

C. STATOR CURRENT BASED MRAS SPEED ESTIMATOR DESIGN

$$\frac{d}{dt}\hat{i}_{s\beta} = \frac{1}{\sigma L_s}(V_{s\beta} - R_s\hat{i}_{s\beta} - \frac{L^2}{L_rT_r} + \frac{L_m}{L_rT_r}\hat{\phi}_{r\beta} + \frac{L_m}{L_r}\hat{\omega}_r\hat{\phi}_{r\alpha}) \tag{13}$$

$$\frac{d}{dt}\hat{i}_{s\alpha} = \frac{1}{\sigma L_s}(V_{s\alpha} - R_s\hat{i}_{s\alpha} - \frac{L^2}{L_rT_r}\hat{i}_{s\alpha} + \frac{L_m}{L_rT_r}\hat{\phi}_{r\alpha} + \frac{L_m}{L_r}\hat{\omega}_r\hat{\phi}_{r\beta}) \tag{14}$$

$$\frac{d}{dt}\hat{\phi}_{r\beta} = \frac{L_m}{L_r}\hat{i}_{s\beta} - \frac{1}{T_r}\hat{\phi}_{r\beta} + \hat{\omega}_r\hat{\phi}_{r\alpha} \tag{15}$$

$$\frac{d}{dt}\hat{\phi}_{r\alpha} = \frac{L_m}{L_r}\hat{i}_{s\alpha} - \frac{1}{T_r}\hat{\phi}_{r\alpha} + \hat{\omega}_r\hat{\phi}_{r\beta} \tag{16}$$

Lyapunov function candidate considered as $V = e^T P_e$

Let $\dot{x} = Ax + B\vec{V}_s$ and $y = Cx$ where system matrix A is written as follows (17)–(22), as shown at the bottom of the page.

Let $\varepsilon_{i\alpha} = i_{\alpha s} - \hat{i}_{\alpha s}$ and $\varepsilon_s = i_s - \hat{i}_s$ Where

$$i_s = \begin{bmatrix}i_{\alpha s} \\ i_{\beta s}\end{bmatrix}$$

$$A = \begin{bmatrix} -\frac{1}{\sigma L_s}(R_s + \frac{L_m^2}{L_rT_r}) & 0 & \frac{1}{\sigma L_s}\frac{L_m}{L_rT_r} & \frac{1}{\sigma L_s}\frac{L_m}{L_r}\hat{\omega}_r \\ 0 & -\frac{1}{\sigma L_s}(R_s + \frac{L_m^2}{L_rT_r}) & -\frac{1}{\sigma L_s}\frac{L_m}{L_r}\hat{\omega}_r & \frac{1}{\sigma L_s}\frac{L_m}{L_rT_r} \\ \frac{L_m}{T_r} & 0 & -\frac{1}{T_r} & \hat{\omega}_r \\ 0 & \frac{L_m}{T_r} & \hat{\omega}_r & -\frac{1}{T_r} \end{bmatrix} \tag{17}$$

$$B = \frac{1}{\sigma L_s}C^T; \tag{18}$$

$$C = \begin{bmatrix}1 & 0 & 0 & 0 \\ 0 & 1 & 0 & 0\end{bmatrix} \tag{19}$$

$$\frac{dv}{dt} = \varepsilon^T\left(A^T + A\right)\varepsilon - 2(\omega_r - \hat{\omega}_r)\left[K\left(\varepsilon_{r\alpha}\hat{\phi}_{r\beta} - \varepsilon_{r\beta}\hat{\phi}_{r\alpha}\frac{1}{r}\frac{d}{dt}\hat{\omega}_r\right)\right] \tag{20}$$

$$\varepsilon^T\left(A^T + A\right)\varepsilon \le Q \tag{21}$$

$$y = C\hat{x} \tag{22}$$

$\varepsilon_{i\beta} = i_{\beta s} - \hat{i}_{\beta s}$ and $\varepsilon_\omega = \omega_r - \hat{\omega}_r$ $V = V_1 + V_2$ Let $V_1 = \varepsilon^T \varepsilon$ and $V_2 = \frac{\varepsilon_\omega^2}{r}$ and the derivative of this Lyapunov candidate function written as $x - \hat{x}$ The derivative of this Lyapunov candidate function written as $Q = \rho I_n$ *and* $\rho \geq 0$ and it is an identity matrix. To prove Lyapunov stability two conditions as to be satisfied (i) The Eigenvalues of the estimator must have negative real parts (ii) The terms factor must be zero i.e., $(\omega_r - \hat{\omega}_r) = 0$

$$K(\varepsilon_\alpha \hat{i}_{s\beta} - \varepsilon_\beta \hat{\phi}_{r\alpha}) - \frac{1}{r}\frac{d}{dt}\omega_r = 0$$
$$\frac{d}{dt}\hat{\omega}_r = rK(\varepsilon_\alpha \hat{\phi}_{r\beta} - \varepsilon_\beta \hat{\phi}_{r\alpha}) \quad (23)$$
$$\hat{\omega}_r = M \int (\varepsilon_\alpha \hat{\phi}_{r\beta} - \varepsilon_\beta \hat{\phi}_{r\alpha}) dt \quad (24)$$

By adjusting the value of M the adaptive law for M is obtained.

$$\hat{\omega}_r = K_i \int \left(\varepsilon_\alpha \hat{\phi}_{r\beta} - \varepsilon_\beta \hat{\phi}_{r\alpha}\right) dt + K_p(\varepsilon_\alpha \hat{\phi}_{r\beta} - \varepsilon_\beta \hat{\phi}_{r\alpha}) dt \quad (25)$$

where *Ki* and *Kp* are adaptive gains for the speed estimator

III. DEVELOPMENT OF MODIFIED BRAIN EMOTIONAL CONTROLLER (MBEC) BASED DTC IM DRIVE

The BEC is developed by extracting the functional process from the limbic system, in which, emotions are generated in the mammalian brain by associating information from different parts, then it sends a response as a specific action. Emotions are basic components that play an important role in human intelligence and decision-making. Sensory cortex, Amygdala, Thalamus and Orbitofrontal cortex are the primary components of the limbic system. The intelligent emotional response is extremely fast compared to traditional control systems; the same comparison is applied to control engineering implementations to illustrate rapid decision making.

The MBEC can be used to control the speed of an IM drive. The Sensory cortex, which analyses sensory signals and sends them to Amygdala and the Orbitofrontal cortex, is used in the modeling of MBEC. The learning weights of the Amygdala and Orbitofrontal cortex are adjusted with the inclusion of the sensory cortex. It can improve in the speeding up of the signal conditioning of Amygdala and Orbitofrontal cortex signals to produce final emotional output whereas in the existing BEC Sensory cortex signals are not available.

In MBEC architecture sensory cortex is included, according to anatomy of brain Sensory cortex is responsible for five major senses namely smell, sound, taste, vision and touch as well as the proprioceptive sensory information. It is to be noted that in the mammalian brain there are distinct and specialized modules for each of the senses and these modules are spatially distributed over the cortical and sub-cortical regions of the brain. For the sake of simplicity we lumped all these senses into a module called Sensory cortex (SC) in the MBEC architecture. The sensory information is integrated with components of the limbic system i.e., amygdala and OFC, to generate necessary action/response in a given task. The inclusion of SC modifies the learning rate of amygdala and OFC and enables processing of information very rapidly and with accuracy.

A. MODELLING OF MODIFIED BRAIN EMOTIONAL CONTROL

The Sensory Cortex (SC_k) and Thalamus in the BEC design, have not been considered in the existing BEC design. The inclusion of SC_k and Thalamus can be modified in this article, so modified BEC can be proposed. The combination of SC_k with the limbic system would improve decision-making by producing sufficient emotional signals, allowing for a quick response. The amygdala and O_k learning mechanisms are modified with SC_k inclusion. A MBEC computational model is made up of sensory input stimuli nodes S_k, sensory cortex nodes SC_k, and thalamus nodes A_{th}. The amygdala is represented by A_k, the orbitofrontal cortex by O_k, and the output node by E. A MBEC computational model made up of sensory input stimuli nodes S_k, sensory cortex nodes S_{ck}, and thalamus nodes A_{th}. The amygdala is represented by A_k, the orbitofrontal cortex by O_k, and the output node by E. Fig. 3 depicts the mechanism of emotional signal output. The controller's feedback is transformed to a sensory signal S_k (26) with the function f, which is then analyzed to produce an emotional signal from the thalamus as

$$S_k = f(e_w, z_c) \quad (26)$$
$$f = K_1 e_w + K_2 . \int z_c dt \quad (27)$$

The thalamus built in this paper is to enable sensory signals to enter the Sensory Cortex SC_k and the amygdala A_k in a superficial manner. In SC_k, the sensory signal is analyzed with function g, and the sensory cortex's output is sent to the Amygdala.

$$SC_k = g(S_k) \quad (28)$$
$$g(S_k) = e^{S_k} \quad (29)$$
$$A_k = S_k V_k \quad (30)$$
$$\Delta V_k = \alpha \max(0, EC - A_k) SC_k \quad (31)$$
$$O_k = W_k S_k \quad (32)$$
$$\Delta W_k = \beta(E' - EC) SC_k \quad (33)$$
$$E' = A_k - O_k \quad (34)$$

Amygdala receives Thalamus, Sensory Cortex and elevated stimulation values as an emotional cue. The model of amygdala learning contains a sensory signal connection. The relationship of amygdala gain is formed by learning rate (α) and emotional cue (EC). The result of the amygdala is helped to resolve the unsuitable and noisy strengthening of the amygdala, which generates the required emotional stimulus for a complete response. The Orbitofrontal Cortex,

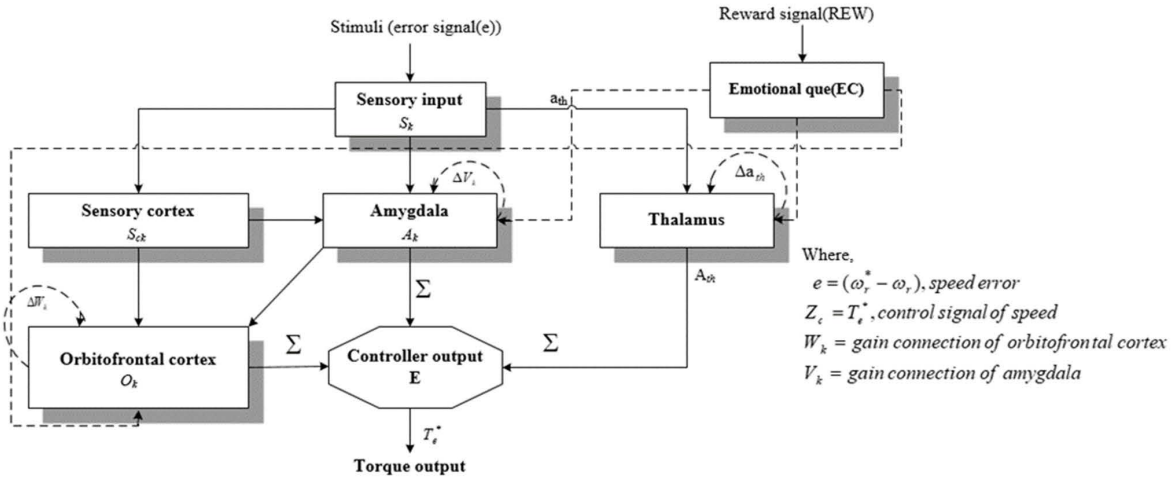

FIGURE 3. Structure of MBEC.

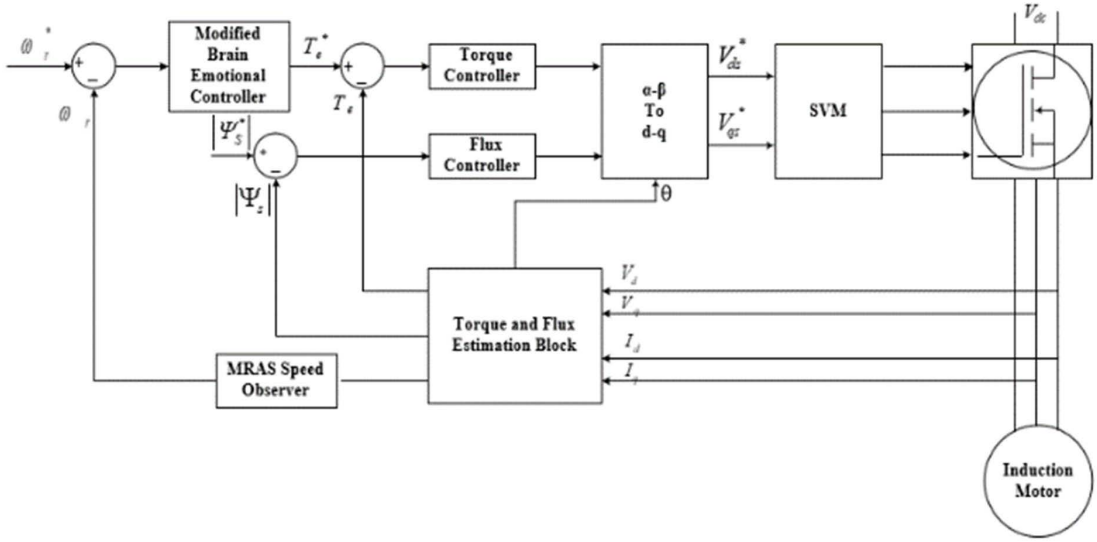

FIGURE 4. MBEC based SVM-DTC of IM drive.

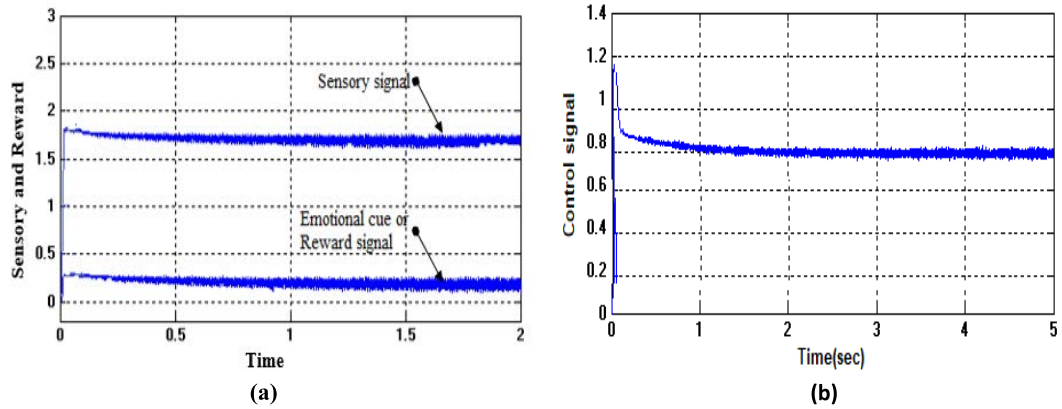

FIGURE 5. Existing BEC characteristics for IM drive (a) Sensory and reward signal (b) control signal.

O_k gets Sensory Cortex input, amygdala input and high emotional indication. The OFC learning model is connected with the β and E' learning rates. The emotional cue is produced by the function h and the emotional signal (36).

$$EC = h(e, z_c) \tag{35}$$

$$E = A - O \tag{36}$$

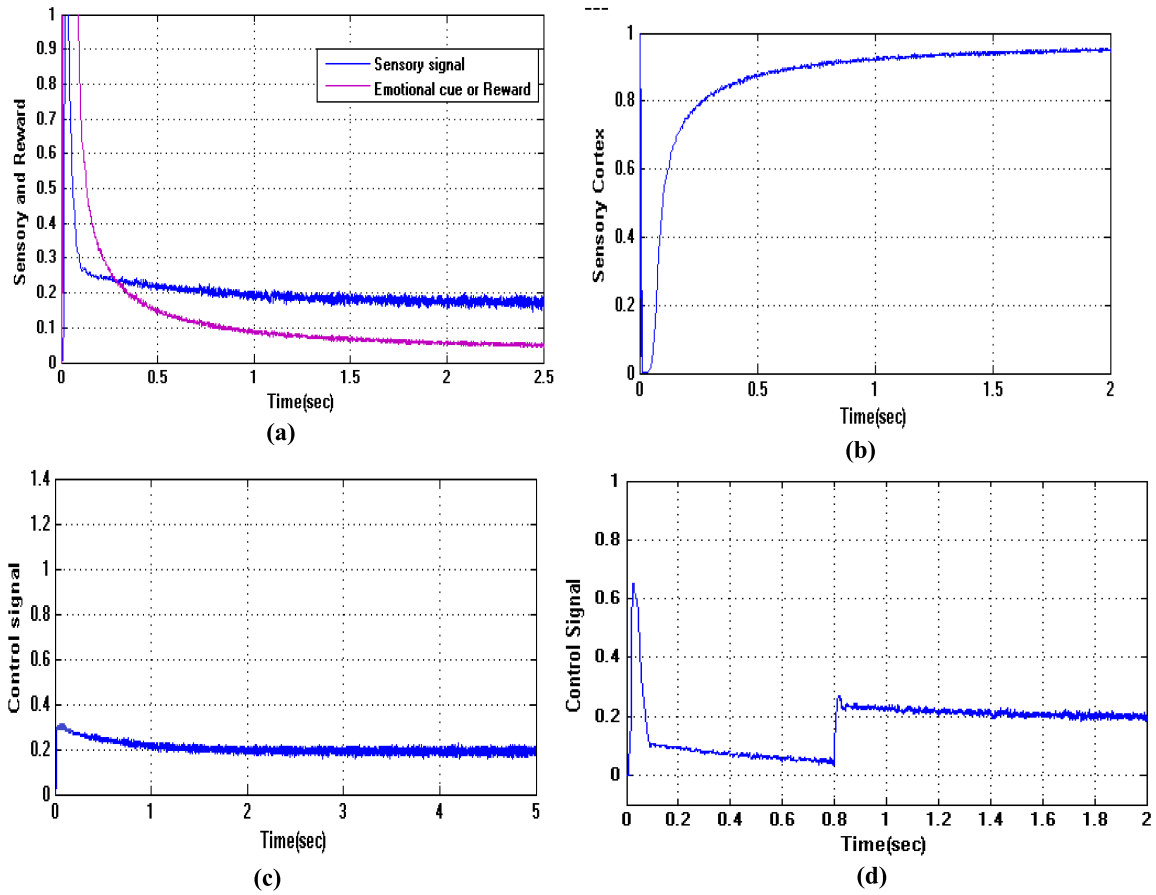

FIGURE 6. Modified BEC characteristics for IM drive (a)Sensory and reward signal (b)Sensory cortex signal (c) Control signal at no load (d) Control signal at full load applied at step time 0.8 sec.

The following algorithm is used to design the MBEC.

Step 1 The BEC architecture begins with the initialization of the sensory stimuli function, S_k as defined in (26). To interact with the amygdala and orbitofrontal cortex, this signal is processed in the sensory cortex and thalamus.

Step 2 In the sensory cortex, the sensory input is evaluated as seen in the functional equation SC_k (28). The signal is then generated and distributed to the amygdala and orbitofrontal cortex.

Step 3 Choosing the correct reward creates a signal link and increases learning in the amygdala and orbitofrontal cortex, enabling you to achieve the optimal response. The signal is sent to the amygdala and orbitofrontal cortex, and its general equation is modeled as in (35).

Step 4 Using equation (30), the amygdala is constructed, and amygdala learning is obtained using reward and learning rate "α" as seen in (31). The amygdala output is always a high value attributable to the maximum term in the learning equation.

Step 5 The reaction of the amygdala, adjusted by the orbitofrontal cortex learning model (32), is modeled with the emotional cue and sensory cortex, with a learning rate of "β", as seen in (33).

Step 6 In the output node, the amygdala and orbitofrontal cortex signals are processed to produce an emotional response using equation (36). If the emotional signal generated corresponds to the desired response of the plant, the process is interrupted otherwise it starts again from step 1.

B. MBEC FOR DTC BASED IM DRIVE

The torque ripple of the DTC motor is predicted to be significant in this paper, thus speed control is made based on the torque error, and it is regarded as an Emotional cue (EC) or reward signal to decrease torque ripples. In Fig.4. shows the block diagram of MBEC based DTC IM drive. The motor speed and the approximate reference torque are the other functions in the incentive. In the reward types, both of these signals are used as adverse feedback from the scheme. Then the stimuli, S_k and emotional cue, EC of this proposed controller as

$$S_k = fe_w \tag{37}$$

$$EC = h(e_t, w_r, z_p) \tag{38}$$

Where,

$$e_\omega = \left(\omega_r^* - \omega_r\right), \quad speed\ error$$

$$e_t = \left(T_e^* - T_e\right), \quad Torque\ error\ from\ DTC\ controller$$

$$\omega_r = Speed\ of\ the\ motor$$

The weighted sensory stimuli, that is input function, f is defined as

$$f = (K_p e_w + K_i \int_0^t e_w dt) \tag{39}$$

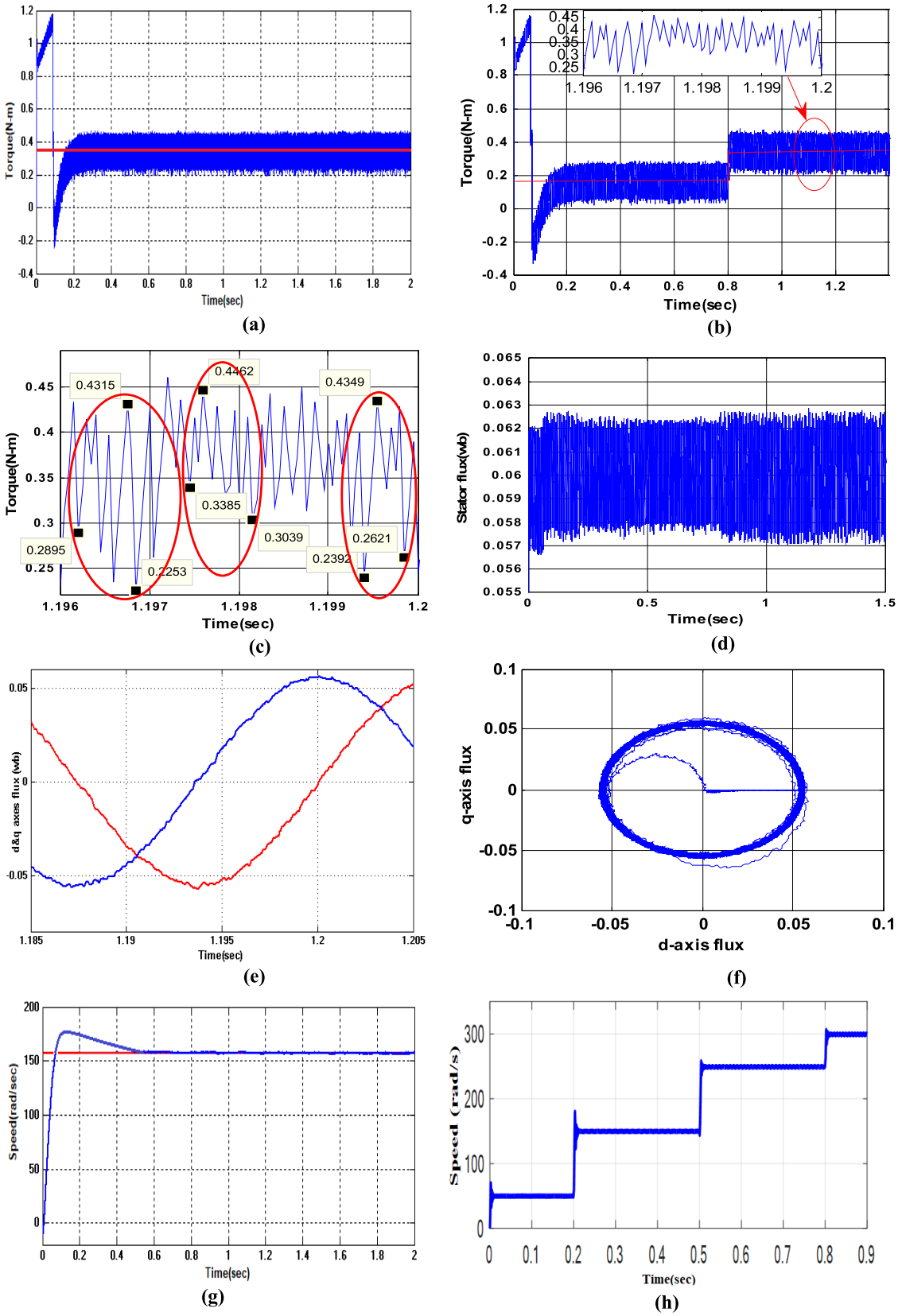

FIGURE 7. Simulation results of PI-based sensorless IM drive under no load condition: Reference speed = 157 rad/sec (a) Torque (g) Speed (h) with different speed. At 0.8 sec, a 0.36 N-m step change in load is applied: (b) Torque (c) Zoomed torque (d) Stator flux (e) d-q axis stator flux (f) d-q axis stator flux locus (i) Speed (j) three phase stator currents.

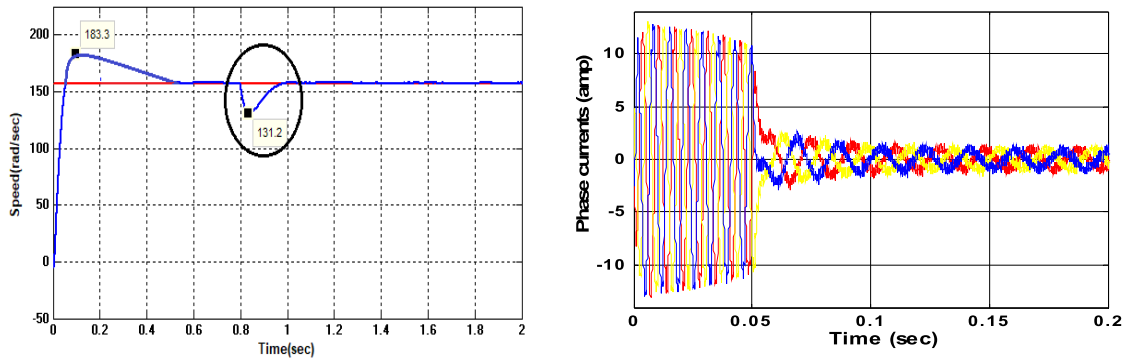

(i) (j)

FIGURE 7. *(Continued.)* **Simulation results of PI-based sensorless IM drive under no load condition: Reference speed = 157 rad/sec (a) Torque (g) Speed (h) with different speed. At 0.8 sec, a 0.36 N-m step change in load is applied: (b) Torque (c) Zoomed torque (d) Stator flux (e) d-q axis stator flux (f) d-q axis stator flux locus (i) Speed (j) three phase stator currents.**

where f is considered as a proportional-integral (PI) function and it has k_p and k_i as its gains and it is used to fine-tune the controller gains by trial and error basis. An online tuning mechanism for controller parameters should be built at every sample time in the design of self-learning-based controllers. As shown in (29), (31) and (32), the predicted reward function controls the self-learning process in MBEC (33). In, DTC torque ripple varies with inverter switching actions. The learning rule in the amygdala as

$$\Delta K_a = K_1 . \max(0, EC - A_o) \geq 0 \tag{40}$$

That k_a represents the weight in the Amygdale link. k_1 is the Amygdala's learning rate, while EC is the Emotional Cue Function or reward signal. In addition, the learning rule in the orbitofrontal cortex

$$\Delta K_{oc} = K_2 . (MO - EC) \tag{41}$$

If (38) and (39) are combined, we have

$$MO = (K_a - K_{oc}) S_i \tag{42}$$

The emotional signal of EC shows that the system is operating well, and it may adjust for both primary and secondary system goals, such as torque ripple reduction. In this work, we consider EC as

$$EC = C_1 . e_w + C_2 . MO + F(torque\ ripple) \tag{43}$$

That C_1 and C_2 are constant.

The gain parameters are assigned on a trial and error basis which are shown in APPENDIX-II.

IV. STABILITY ANALYSIS OF MRAS

The mechanical model of the system at stationary reference frame is as follows

$$\frac{d}{dt}\hat{\omega}_r = \frac{3\rho L_m}{4JL_r}(\Psi_{\alpha r} i_{\beta s} - \Psi_{\beta r} i_{\alpha s}) - \frac{f}{J}\omega_r - \frac{f}{J} \tag{44}$$

Using small signal analysis

$$\Delta y = c\Delta x = (SI - A)^{-1} \Delta A x_o \tag{45}$$

$$\Delta \dot{x} = A\Delta x + \Delta A x_o \text{ where } \Delta x = \left(x - \hat{x}\right) \text{ and}$$
$$x_o = [i_{ds0} \quad i_{qs0} \quad \phi_{dr0} \quad \phi_{qr0}]^T \tag{46}$$

The system matrix A is expressed as

$$\Delta A = \begin{bmatrix} 0 & 0 & 0 & a \\ 0 & 0 & -a & 0 \\ 0 & 0 & 0 & -1 \\ 0 & 0 & 1 & 0 \end{bmatrix} \Delta\omega_r$$

where

$$a = \frac{1}{\sigma L_s}\frac{L_m}{L_r} \tag{47}$$

$$\Delta y = \begin{bmatrix} i_{\alpha s} & -\hat{i}_{\alpha s} \\ i_{\beta s} & -\hat{i}_{\beta s} \end{bmatrix} \tag{48}$$

$$adj(SI - A) = \begin{bmatrix} a_{11} & a_{12} & a_{13} & a_{14} \\ a_{21} & a_{22} & a_{23} & a_{24} \\ a_{31} & a_{32} & a_{33} & a_{34} \\ a_{41} & a_{42} & a_{43} & a_{44} \end{bmatrix} \tag{49}$$

$$\begin{bmatrix} \frac{\Delta i_{as}}{\Delta\omega_r} \\ \frac{\Delta i_{\beta s}}{\Delta\omega_r} \end{bmatrix} = C\,(SI - A)^{-1} \begin{bmatrix} 0 & 0 & 0 & a \\ 0 & 0 & -a & 0 \\ 0 & 0 & 0 & -1 \\ 0 & 0 & 1 & 0 \end{bmatrix} \times [i_{ds0} \quad i_{qs0} \quad \phi_{dr0} \quad \phi_{qr0}]^T \tag{50}$$

substitute (49) into (50) and solve from the mechanical model the transfer function of the machine $\varepsilon(s)$ obtained. From equation(49) and the adj of (SI-A)

$$\varepsilon = -\frac{(a_{24} - a_{22})}{|SI - A|}\hat{\Psi}_{\alpha r0}\Delta\omega_r$$
$$\frac{\varepsilon(s)}{m(s)} = \left\{ -\frac{(a_{24} - a_{22})}{|SI - A|}\frac{1}{CS + f(j)}\frac{p}{2j}\hat{\phi}^2_{\alpha r0} \right\}$$
$$\frac{\omega_r}{\hat{\omega}_r} = \left\{ \frac{(G_{(s)}(K_{Pmras} + (K_{Imras}/s)))}{1 + (G_{(s)}(K_{Pmras} + (K_{Imras}/s)))} \right\}$$

V. IMPLEMENTATION OF SVM DTC IM DRIVE USING MBEC

In order to validate the proposed method, let us consider the parameter as given in Appendix – I. The overall MBEC based

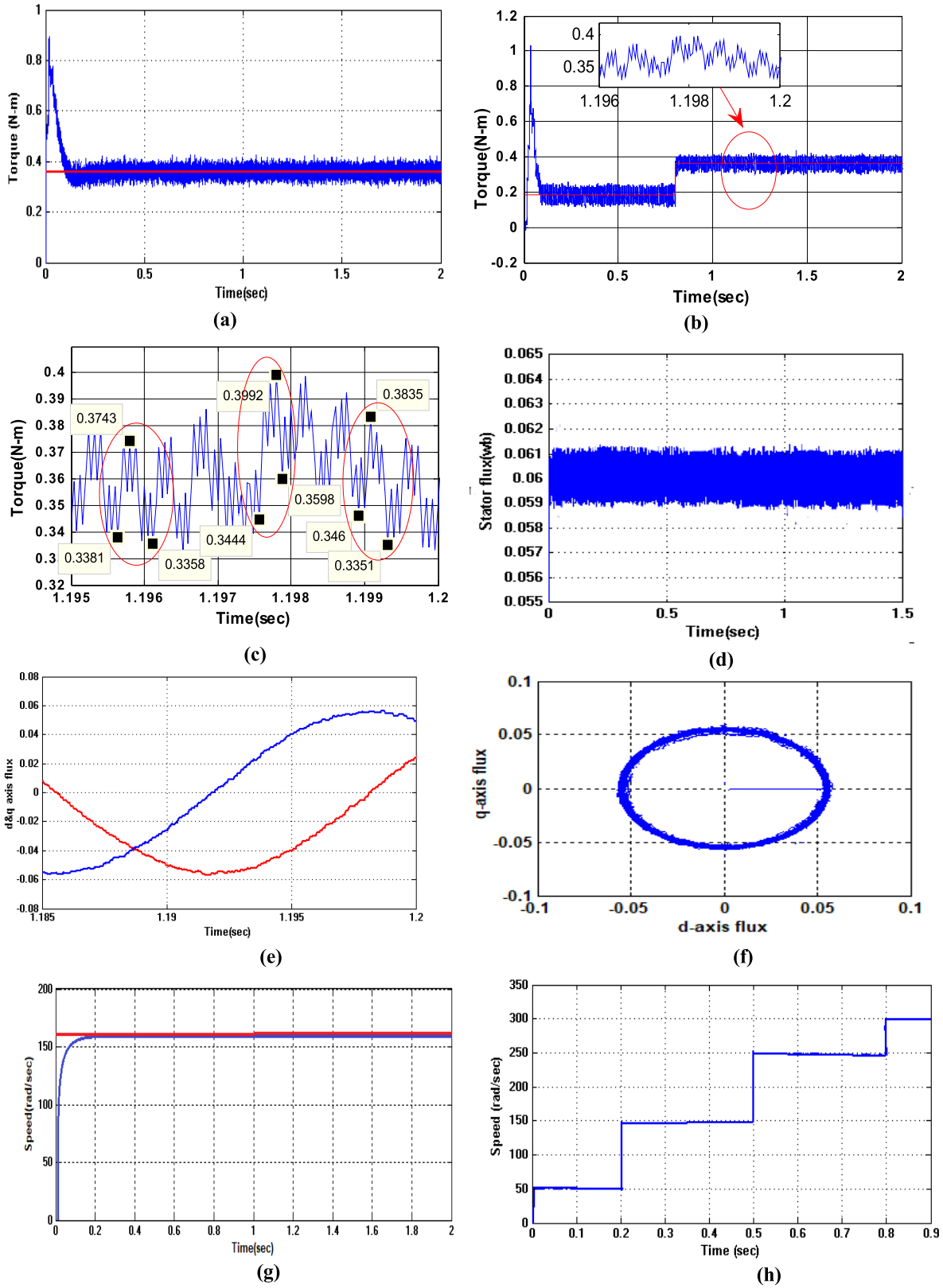

FIGURE 8. Simulation results of MBEC based sensorless IM drive under no-load condition. The reference speed = 157 rad/sec (a) Torque, (g) Speed, (h) with different speed tracking. At 0.8 sec, a 0.36 N-m step change in load is applied: (b) Torque (c) Zoomed torque (d) Stator flux (e) d-q axes stator flux (f) d-q axis stator flux locus (i) Speed (j) Estimated speed with MRAS (k) Three phase stator currents (l) Phase voltages.

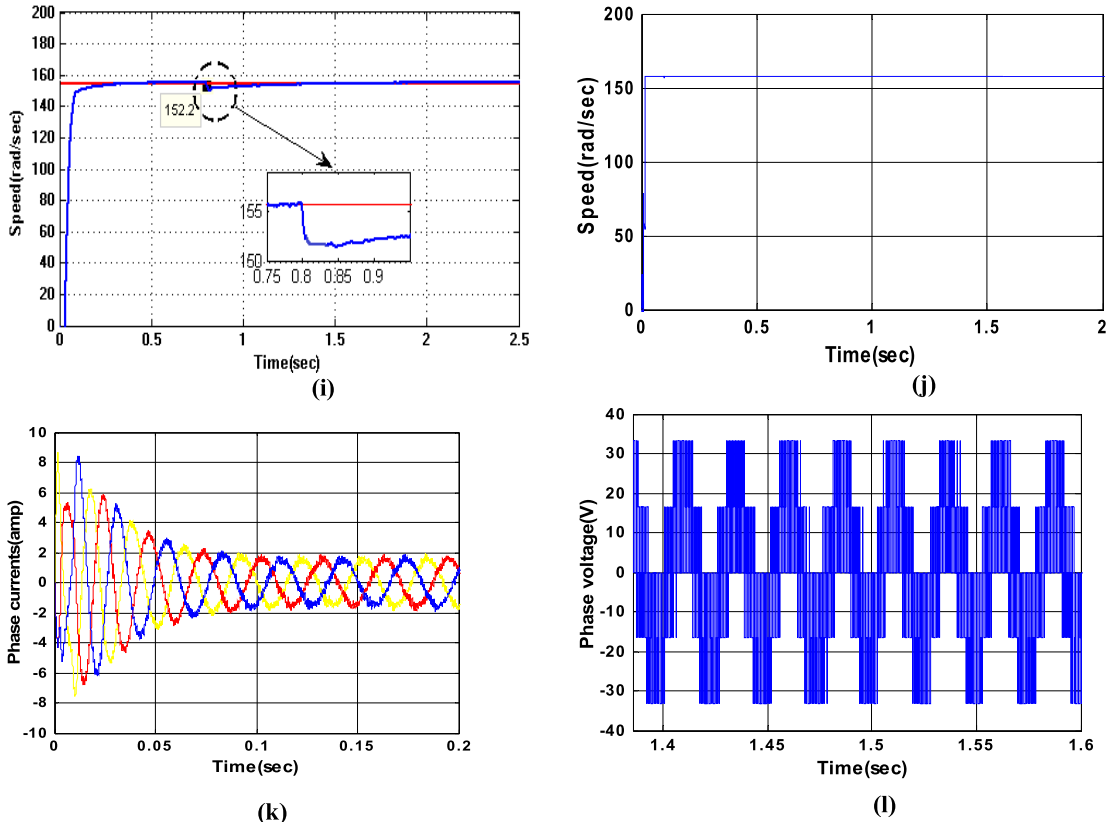

FIGURE 8. *(Continued.)* **Simulation results of MBEC based sensorless IM drive under no-load condition. The reference speed = 157 rad/sec (a) Torque, (g) Speed, (h) with different speed tracking. At 0.8 sec, a 0.36 N-m step change in load is applied: (b) Torque (c) Zoomed torque (d) Stator flux (e) d-q axes stator flux (f) d-q axis stator flux locus (i) Speed (j) Estimated speed with MRAS (k) Three phase stator currents (l) Phase voltages.**

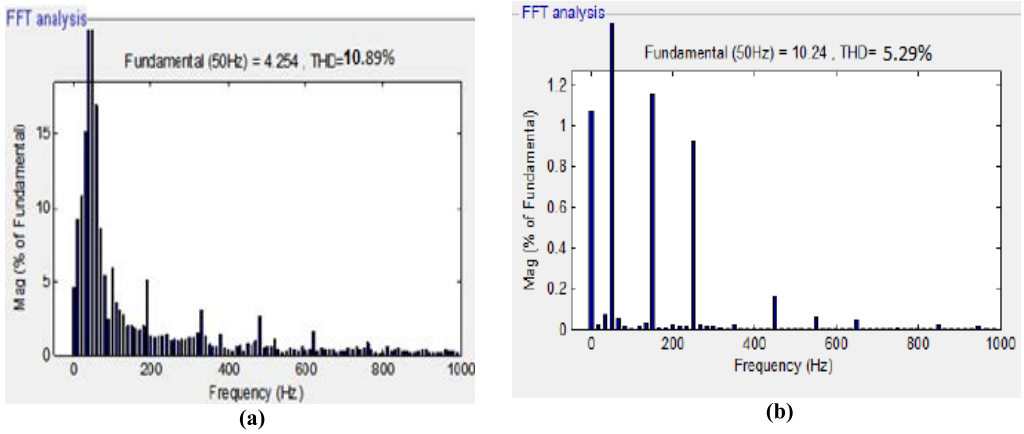

FIGURE 9. **Frequency spectrum analysis of stator current using (a) MBEC based IM drive (b) PI based IM drive.**

DTC motor drive is shown in Fig. 4. The proposed method is implemented through simulation and validated through experimentation. The performance of the proposed scheme is presented in the following subsections.

A. SIMULATION RESULTS

The performance of the existing BEC and MBEC are presented in Fig. 5(a), 5(b) and Fig. 6(a), 6(b), 6(c) respectively. It can be seen from the figures that the reaction of the sensory input signal is reduced to a considerable level. As compared to the MBEC, the sensory signal value in the existing BEC is extremely high, which has an impact on the system's overall performance. The incorporation of sensory cortex signal to the MBEC decreased the scale of the amygdala and OFC learning models in comparison to the existing BEC design. As a result, the characteristics show that MBEC can minimize signal processing when compared to BEC. The simulation findings were achieved using a 157 rad/sec speed reference

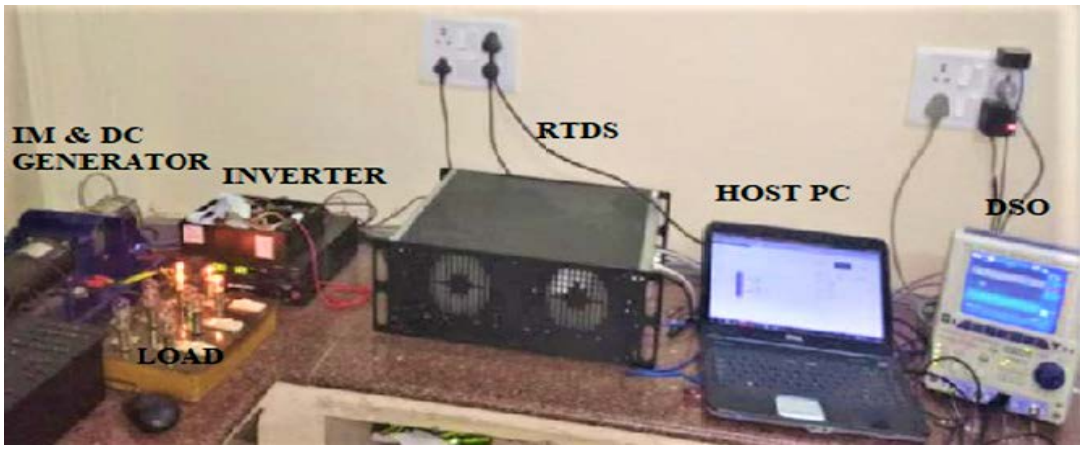

FIGURE 10. RCP based experimental setup photograph for SVM DTC IM drive.

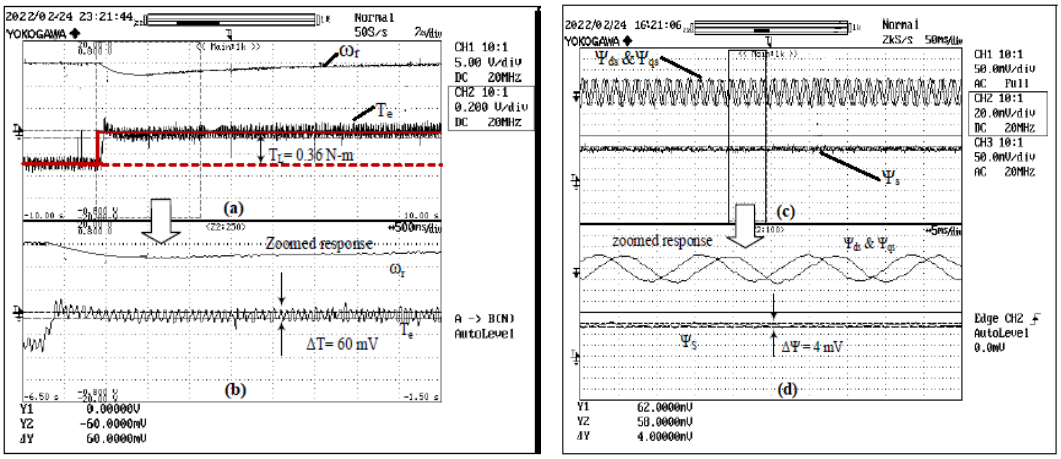

FIGURE 11. Simulated MBEC based sensorless IM drive in RT-LAB HIL setup (a) Speed and Torque, (b) Zooming output of speed and Torque, (c) d-q axes flux, (d) stator flux.

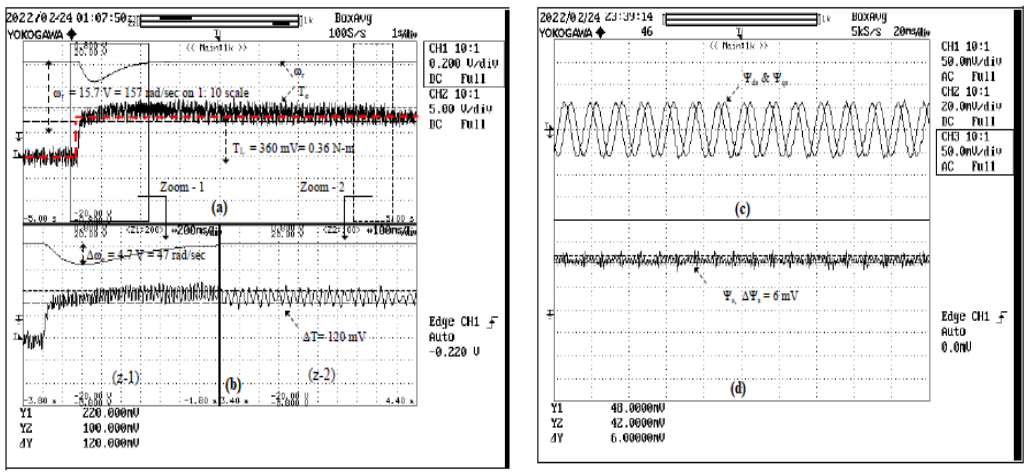

FIGURE 12. Simulated PI based sensorless IM drive in RT-LAB HIL setup (a) Speed and Torque (b) Zooming output of speed and Torque (c) d-q axes flux (d) stator flux.

and a 0.36 N-m load step change at a step duration of 0.8 sec. The torque response and its snapshot of the zoomed response of PI and MBEC base SVM DTC strategy are observed in Fig. 7(a), 7(b), 7(c) and Fig. 8(a), 8(b), 8(c). The T_{max} and T_{min} are noted at the 1.2-second simulation period when the torque ripple of SVM DTC is computed. The torque ripple is determined using the averaging approach (51), as indicated in the zooming response of the torque ripple for

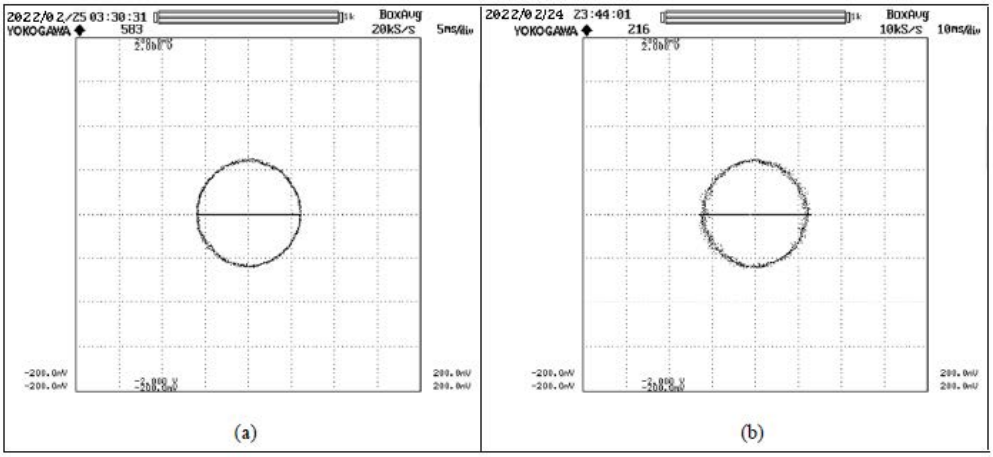

FIGURE 13. Simulated sensorless IM drive in RT-LAB HIL setup (a) d-q axis flux locus of MBEC based SVM DTC strategy, (b) d-q axis flux locus of PI-based SVM DTC strategy.

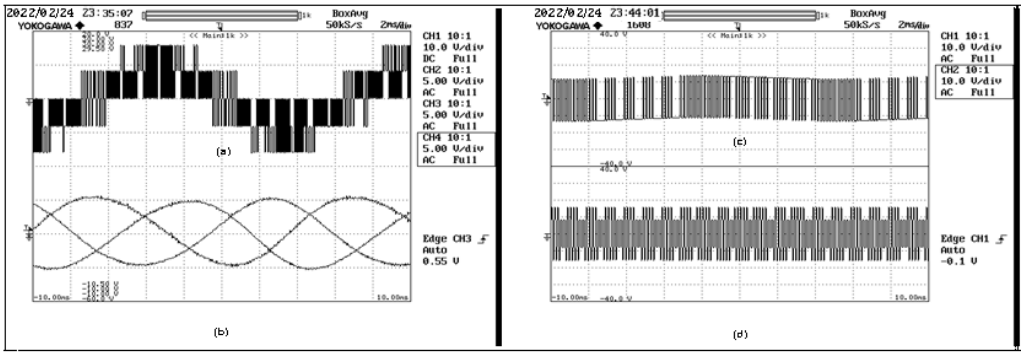

FIGURE 14. Simulated MBEC based sensorless IM drive in RT-LAB HIL setup (a) phase voltage on 1:2 scale (b) stator currents (c) pole voltage on 1:2 scale and (d) common-mode voltage.

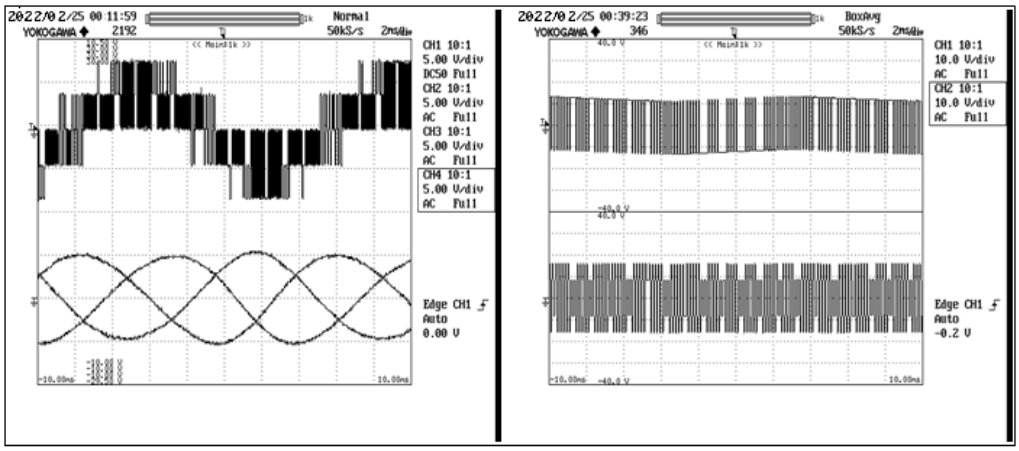

FIGURE 15. Simulated PI based sensorless IM drive in RT-LAB HIL setup (a) phase voltage on 1:2 scale (b) stator currents (c) pole voltage on 1:2 scale and (d) common-mode voltage.

three sets of data tips. The torque ripple is calculated by the averaging method as expressed (51), shown at the bottom of the page.

Compared with MBEC-based SVM DTC with PI-based DTC, fewer torque ripples are observed. These are shown in Fig. 7 (d), 7 (e), 7 (f) and 8 (d), 8 (e), 8 (f) respectively. The

$$\%\Delta T = \frac{1}{N}\left[\frac{T_{\max 1} - T_{\min 1}}{T_L} + \frac{T_{\max 2} - T_{min2}}{T_L} + \ldots + \frac{T_{\max N} - T_{\min N}}{T_L}\right] \times 100 \tag{51}$$

TABLE 1. Comparative results.

Controller	Performance Parameter	Speed Settling time	Torque ripple(%)	Flux ripple (%)	THD(%)
PI based SVM DTC	Simulation	0.6	14.8	10.9	10.89
	Experimental (Opal-RT HIL RCP)	1.5	15.6	12	13.47
MBEC based SVM DTC	Simulation	0.1	7.89	6.5	5.29
	Experimental (Opal-RT HIL RCP)	0.9	9.29	7.8	8.24

flux ripple for the MBEC controller is 6.0% and for the PI controller, it's 10.9%. MBEC based SVM DTC reduces flux ripple compared to a PI controller.

The MBEC settles smoothly and without oscillations at 157 rad/s with no load, as illustrated in Fig.8(g). When employing PI controller speed, the command speed with transient oscillations is obtained in Fig.7(g). With MBEC and PI controllers, the motor speed achieves its steady state in 0.1 and 0.6 seconds, respectively. On MBEC based IM drives, speed tracking capabilities are tested. Fig. 8(h) shows that the speed of IM is tracking with command speed values of 50-150-250-300 rad/sec at intervals of 0-0.2-0.5-0.8-1 sec. The SVM DTC of the IM drive exhibits a minor fall in speed response when a rapid load is given to the MBEC and PI controller-based SVM DTC in Fig.8(i) shows the load disturbance that occurred at 0.36 N-M at step time of 0.8 sec is shown in Fig.8(i), and Fig.7(i) MBEC is able to rapidly recover the command speed. Fig.8(j) indicates the effects at a constant speed, there are some oscillations during a start in both the real and estimated speeds and the stator phase currents at startup draw a lot of current. The actual and approximate positions of the rotor are paired. The three-phase currents and voltages of both the MBEC and PI control based DTC SVMs are shown in Fig. 7(j), 8(k), and 8(l). From Fig.9(a),9(b) frequency spectrum of stator current, it can be seen that the current waveform in MBEC has less harmonic distortion than the current waveform in the PI controller. According to the figures below, MBEC provides better performance in all conditions, with a fast response, low steady-state error, and sensitivity to the disturbing load. Torque and flux ripples were minimized as well. The MBEC overcomes the problems.

B. EXPERIMENTAL RESULTS

Experimental efficiency investigation of proposed MBEC based SVM DTC technique for IM is performed by utilizing Op-RTDS. The performance results are comparable to PI based SVM DTC method. The Op-RTDS is used in the hardware-in-loop (HIL) [28] mechanism, which creates closed loop access in real time between plant and control algorithms, and this type of configuration is known as rapid control prototyping (RCP) [29], [30]. Using an RCP-based experimental setup, the difficulties associated with fast processing micro controllers and DSPs are removed, and a reconfigurable system for validating control methods is created. HIL is used to access DTC signals from the mathematical Simulink model as well as plant control signals. The OP5142 FPGA card in Op-RTDS collects and executes PWM operations on high-speed analog/digital signals. Soft-line computed Simulink PWM signals are transformed into power signals in real-time by the OP5142 FPGA card in this task. The Op-RTDS is equipped with a multicore power PC. The simulink.mdl computations are executed in one of these cores. The Op-RTDS and the host PC are linked in the hand-shake mode, as seen in Fig. 10. The experimental photograph. The experimental results of speed, torque and flux response of MBEC and PI based DTC SVM of IM drive with a reference speed of 157 rad/sec are shown in Fig. 11(a), 11(c) and 12(a), 12(c). A D.C generator is linked to a reasonable number of bulbs as the drive's load. Fig. 11(b), 11(d), and 12(b), 12(d) show the rpm, torque, and flux responses of the IM drive's loaded-condition MBEC-based SVM-DTC. Outgoing op-RTDS channels are used to calculate the magnitude of speed and torque in voltage terms. By observation, the actual torque ripple corresponding to this 100mv is equal to 9.29 % under loaded conditions when calculated using (51) The torque ripple is 15.6 % when using a PI controller, as seen in Fig. 12(a), (b). On a 1:10 ratio, the voltage corresponding to the decrease in speed is 0.7 V. The real speed droop is $0.7 \times 10 = 7$ rad/sec in this case. The d-q axis flux locus of both MBEC and PI controller based SVM DTC is shown in Fig. 13(a), 13(b). The three-phase voltages and three-phase currents are shown in Fig. 14(a), 14(b), 14(c), 14(d).

The performance of SVM-DTC IM drive is shown in Table 1, with PI controller and MBEC in terms of speed settling time, torque ripples, flux ripples and stator currents THD respectively. The speed settling time with

PI based IM drive is 0.6s in simulation and 1.5s in real-time experimentation whereas MBEC is recorded as 0.1s in simulation environment and 0.9s in experimentation. Torque ripples and flux ripples with PI based drive are recorded as 14.8% and 10.9% as against to 7.89% and 6.9% in MBEC based drive in simulation environment. In real-time experimentation 15.6% of torque ripples and 12% of flux ripples are recorded for PI based drive and with MBEC based drive torque and flux ripples recorded as 9.29% and 8%. The stator currents THDs are 10.89% for PI based drive and 5.29% for MBEC based drive in simulation results. In real-time stator currents THD is recorded as 13.47% for PI based drive and 8.24% for MBEC based drive. The results shows that the MBEC based IM drive gives high performance compared to PI based drive in terms of fast settling time, less ripples in flux and torque and lesser THD in stator currents.

VI. CONCLUSION

In this paper a modified brain emotional controller is presented. It is inferred that this MBEC is very well adaptive for tuning parameters and shows good self-learning mechanism. The proposed controller is used for SVM based DTC of induction motor drive, an efficient MBEC is used to control the speed and ripple minimization of torque and flux of sensorless IM drive. The effectiveness of MBEC is tested in simulation environment and implemented in the Op-RTDS and experimental results are analyzed. MBEC controller achieves dynamic performance in terms of less settling time without any reduced peak over shoots and significantly decreases torque and flux ripples when compared with PI controller.

APPENDIX–I

Parameters of Induction Motor:

Rating: Parameters:

$$P_s = 120W, \quad V_s = 36V, \quad R_s = 0.896\Omega,$$
$$L_{ls} = 1.94mH, \quad 3\Phi - AC \quad f = 120Hz \quad R_r = 1.82\Omega,$$
$$L_{lr} = 2.45\,mH, \quad I_s = 6\text{A}, \quad P = 4 \quad L_m = 69.3mH$$

APPENDIX–II

Parameters of BEC

$\alpha = 0.005\ \beta = 0.002$

Sensory signal gain parameters $= 0.0455, 2 \times 10^{-3}, 6 \times 10^{-2}$.

Emotional signal gain parameters $= 3.4\times10^{-2}, 4.8\times10^{-3}, 1 \times 10^{-3}$.

Speed signal gain $= 0.05$

Control signal gain $= 0.09$

APPENDIX-III

Stability analysis of Induction Motor

The transfer function of the Induction motor is represented as

$$\frac{\theta_s}{V_a(s)} = \frac{K_a}{JL_aS^3 + (R_aJ + BL_a)\,S^2 + (BR_a + K_aK_t)S} \tag{A.1}$$

The motor parameters in Appendix-I is substituted in Equation (A.1) Where

$$K_a = \frac{3}{2\pi n_s} = 0.000318$$
$$n_s = \frac{120f}{p} = 1500$$
$$J\ (\text{Inertia constant}) = 0.225e^{-3} = 0.01120$$
$$L_a = 1.5394,$$
$$R_a = 1.82,$$
$$K_t = 0.5$$
$$\textit{Transfer function gives}\frac{\theta_s}{V_a(s)}$$
$$= \frac{0.000318}{0.172S^3 + 0.0203S^2 + 0.0001579}$$
$$= \frac{0.000318}{S(S + 0.00788))(S + 1.172)} \tag{A.2}$$
$$G\,(s) = \frac{0.03443}{S(1 + 126.9S)(S + 0.53S)} \tag{A.3}$$
$$G\,(s) = \frac{0.03443}{108.24S^3 + 127.75S^2 + S + 0} \tag{A.4}$$

The root locus is drawn for (A.4) and found that the plots of induction motor are at left hand side of the R-H plane shown in Fig. 16.

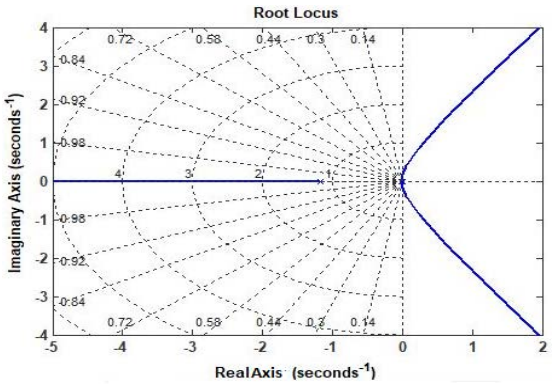

FIGURE 16. Root locus diagram of IM.

REFERENCES

[1] C. Lucas, R. M. Milasi, and B. N. Araabi, "Intelligent modeling and control of washing machine using locally linear neuro-fuzzy (LLNF) modeling and modified brain emotional learning based intelligent controller (BELBIC)," *Asian J. Control*, vol. 8, no. 4, pp. 393–400, Oct. 2008.

[2] M. Qutubuddin, T. K. Gibo, R. S. Bapi, and Y. Narri, "Brain affective system inspired control architecture: An application to nonlinear system," *IEEE Access*, vol. 9, pp. 86565–86580, 2021.

[3] S. Ale Aghaee, C. Lucas, and K. Amiri Zadeh, "Applying brain emotional learning based intelligent controller (BELBIC) to multiple-area power systems," *Asian J. Control*, vol. 14, no. 6, pp. 1580–1588, Nov. 2012.

[4] A. R. Mehrabian, C. Lucas, and J. Roshanian, "Aerospace launch vehicle control: An intelligent adaptive approach," *Aerosp. Sci. Technol.*, vol. 10, no. 2, pp. 149–155, Mar. 2006.

[5] B. Debnath and S. J. Mija, "Adaptive emotional-learning-based controller: A practical design approach for helicopters with variable speed rotors," *IEEE Trans. Ind. Informat.*, vol. 18, no. 2, pp. 1132–1141, Feb. 2022.

[6] D. Casadei, F. Profumo, G. Serra, and A. Tani, "FOC and DTC: Two viable schemes for induction motors torque control," *IEEE Trans. Power Electron.*, vol. 17, no. 5, pp. 779–787, Sep. 2002.
[7] I. Takahashi and T. Noguchi, "A new quick-response and high-efficiency control strategy of an induction motor," *IEEE Trans. Ind. Appl.*, vol. IA-22, no. 5, pp. 820–827, Sep. 1986.
[8] G. S. Buja and M. P. Kazmierkowski, "Direct torque control of PWM inverter-fed AC motors—A survey," *IEEE Trans. Ind. Electron.*, vol. 51, no. 4, pp. 744–757, Aug. 2004.
[9] T. G. Habetler, F. Profumo, M. Pastorelli, and L. M. Tolbert, "Direct torque control of induction machines using space vector modulation," *IEEE Trans. Ind. Appl.*, vol. 28, no. 5, pp. 1045–1053, Sep. 1992.
[10] C. Lascu, I. Boldea, and F. Blaabjerg, "A modified direct torque control for induction motor sensorless drive," *IEEE Trans. Ind. Appl.*, vol. 36, no. 1, pp. 122–130, Jan./Feb. 2000.
[11] A. Tripathi, A. M. Khambadkone, and S. K. Panda, "Torque ripple analysis and dynamic performance of a space vector modulation based control method for AC-drives," *IEEE Trans. Power Electron.*, vol. 20, no. 2, pp. 485–492, Mar. 2005.
[12] S. El Daoudi, L. Lazrak, and M. Ait Lafkih, "Sliding mode approach applied to sensorless direct torque control of cage asynchronous motor via multi-level inverter," *Protection Control Mod. Power Syst.*, vol. 5, no. 1, p. 13, Dec. 2020.
[13] M. R. Khan, A. Iqbal, and M. Ahmad, "MRAS-based sensorless control of a vector controlled five-phase induction motor drive," *Electr. Power Syst. Res.*, vol. 78, no. 8, pp. 1311–1321, Aug. 2008.
[14] M. R. Khan and I. Iqbal, "MRAS based sensorless control of a series-connected five-phase two-motor drive system," *J. Elect. Eng. Technol.*, vol. 3, no. 2, pp. 224–234, 2008.
[15] C. U. Reddy, K. K. Prabhakar, A. K. Singh, and P. Kumar, "Speed estimation technique using modified stator current error-based MRAS for direct torque controlled induction motor drives," *IEEE J. Emerg. Sel. Topics Power Electron.*, vol. 8, no. 2, pp. 1223–1235, Jun. 2020.
[16] C. Lucas, D. Shahmirzadi, and N. Sheikholeslami, "Introducing BELBIC: Brain emotional learning based intelligent controller," *Intell. Automat. Soft Comput.*, vol. 10, no. 1, pp. 11–22, 2004.
[17] J. Moren, "Emotional learning: A computational model of the Amygdala," *Cybern. Syst.*, vol. 32, pp.611-636, Mar. 2001.
[18] J. Moren and C. Balkenius, "A computational model of emotional learning in the Amygdala," in *Proc. 6th Int. Conf. Simulation Adapt. Behav.*, Cambridge, MA, USA, 2000, pp. 411–436.
[19] Z. Beheshi and S. Z. Md Hashim, "A review of emotional learning and it's utilization in control engineering," *Int. J. Advance Soft Comput. Appl.*, vol. 2, no. 2, pp. 191–208, Jul. 2010.
[20] J.-J. E. Slotine W. Li, *Applied Nonlinear Control*. Englewood Cliffs, NJ, USA: Prentice-Hall, 1991.
[21] M. Qutubuddin and N. Yadaiah, "Performance evaluation of neurobiologically inspired brain emotional adaptive mechanism for permanent magnet synchronous motor drive," *Arabian J. Sci. Eng.*, vol. 47, pp. 3181–3199, 2022, doi: 10.1007/s13369-021-06111-7.
[22] A. Khedher and M. Faouzi Mimouni, "Sensorless-adaptive DTC of double star induction motor," *Energy Convers. Manage.*, vol. 51, no. 12, pp. 2878–2892, Dec. 2010.
[23] C. M. F. S. Reza, M. D. Islam, and S. Mekhilef, "A review of reliable and energy efficient direct torque controlled induction motor drives," *Renew. Sustain. Energy Rev.*, vol. 37, pp. 919–932, Sep. 2014.
[24] E. Daryabeigi, A. Mirzaei, H. Abootorabi Zarchi, and S. Vaez-Zadeh, "Enhanced emotional and speed deviation control of synchronous reluctance motor drives," *IEEE Trans. Energy Convers.*, vol. 34, no. 2, pp. 604–612, Jun. 2019.
[25] A. Verma, B. Singh, and D. Yadav, "Investigation of ANN tuned PI speed controller of a modified DTC induction motor drive," in *Proc. IEEE Int. Conf. Power Electron., Drives Energy Syst. (PEDES)*, Dec. 2014, pp. 1–6.
[26] C. Lucena, L. Palma, A. Cardoso, and P. Gil, "Optimal gains tuning of PI-fuzzy controllers," in *Proc. 20th Medit. Conf. Control Automat. (MED)*, Jul. 2012, pp. 824–829.
[27] J. Silva, R. Aquino, A. Ferreira, and D. Marques, "Deep brain emotional learning-based intelligent controller applied to an inverted pendulum system," *J. Supercomput.*, vol. 78, no. 6, pp. 8346–8366, Apr. 2022, doi: 10.1007/s11227-021-04200-w.
[28] F. Mak, R. Sundaram, V. Santhaseelan, and S. Tandle, "Laboratory set-up for real-time study of electric drives with integrated interfaces for test and measurement," in *Proc. 38th Annu. Frontiers Educ. Conf.*, Saratoga Springs, NY, USA, Oct. 2008, p. T3H-1.
[29] S. Abourida and J. Belanger, "Real-time platform for the control prototyping and simulation of power electronics and motor drives," in *Proc. 3rd Int. Conf. Modeling, Simulation Appl. Optim.*, Sarjah, United Arab Emirates, 2009, pp. 1–6.
[30] Y. Zhang, P. Huang, and H. Yang, "Hardware-in-the-loop real-time simulation for speed-sensorless vector control of high-power induction motor," in *Proc. 22nd Int. Conf. Elect. Mach. Syst. (ICEMS)*, Aug. 2019, pp. 1–5, doi: 10.1109/ICEMS.2019.8922220.

SRIDHAR SAVARAPU (Senior Member, IEEE) received the B.Tech. and M.Tech. degrees in electrical engineering from the JNTUH College of Engineering Hyderabad, in 2003 and 2006, respectively. He is currently an Assistant Professor with the Department of Electrical and Electronics Engineering, Jawaharlal Nehru Technological University College of Engineering, Anantapur, India. He is the author or coauthor of more than 40 papers in international journals and conferences. His research interests include power electronics, ac drives, and fuzzy logic. He is a member of the Institution of Engineers (India). He is also a reviewer of Elsevier and Springer journals.

MD. QUTUBUDDIN received the B.Tech. degree in electrical and electronics engineering and the M.Tech. and Ph.D. degrees in power electronics from JNTUH Hyderabad, in 2008, 2012, and 2019, respectively. He worked as a Senior Research Fellow with JNTUH Hyderabad. He has five years of research experience and five years of teaching experience. He is currently working as an Assistant Professor with the TKR College of Engineering and Technology, Hyderabad. His research interests include artificial techniques, electrical drives, and cognitive modeling.

YADAIAH NARRI (Senior Member, IEEE) received the B.E. degree in electrical engineering from Osmania University, in 1988, the M.Tech. degree in control systems from the IIT, Kharagpur, India, in 1991, and the Ph.D. degree from JNTU, Hyderabad, India, in 2000. He visited as a Visiting Professor with the University of Alberta, Edmonton, AB, Canada. He is currently a Professor of EEE with Jawaharlal Nehru Technological University Hyderabad, India. He has 145 publications to his credit. He has completed three research and development projects and delivered more than 50 guest lectures as key notes speaker. His research interests include adaptive control, artificial neural networks, fuzzy logic, nonlinear systems, and process control. He is a fellow of the Institution of Engineers (India) and the Institution of Electronics and Telecommunications Engineers. He is a Life Member of the Systems Society of India and the Indian Society for Technical Education. He is an Editorial Board Member of the *Journal of Computer Science* (India). He was awarded 43rd SSI National Systems Gold Medal in 2019, by the Systems Society of India. He was a recipient of the Meritorious State Teacher Award by the Government of Telangana in the year 2015, the Engineer of Year Award - 2014 of the Institution of Engineers of India by Andhra Pradesh Chapter, and the Outstanding Reviewer Award of 2014 by Elsevier Publisher, USA. He was awarded the Young Scientist Fellowship (YSF) of Andhra Pradesh State Council for Science and Technology in 1999.